^{64}Ni+^{64}Ni fusion reaction calculated with the density-constrained time-dependent Hartree-Fock formalism

A. S. Umar and V. E. Oberacker
Department of Physics and Astronomy, Vanderbilt University, Nashville, Tennessee 37235, USA
(Received 25 September 2007; revised manuscript received 24 April 2008; published 9 June 2008)

We study fusion reactions of the ^{64}Ni+^{64}Ni system using the density-constrained time-dependent Hartree-Fock (TDHF) formalism. In this formalism the fusion barriers are directly obtained from TDHF dynamics. In addition, we incorporate the entrance channel alignments of the slightly deformed (oblate) ^{64}Ni nuclei resulting from dynamical Coulomb excitation. We show that alignment leads to a fusion barrier distribution and alters the naive picture for defining which energies are actually sub-barrier. We also show that core orientation effects could play a significant role in fusion cross section calculations.

DOI: 10.1103/PhysRevC.77.064605 PACS number(s): 21.60.Jz, 25.70.Jj

I. INTRODUCTION

Radioactive ion-beam facilities enable us to study the structure and reactions of exotic nuclei, in particular the physics properties of the "terra incognita" of neutron-rich isotopes [1]. One important aspect of these studies is a detailed investigation of the heavy-ion fusion process of exotic nuclei. Not only is this crucial for superheavy element formation, but it will also lead to a better understanding of the effective N-N interactions in neutron-rich nuclei and of enhanced correlations present in these many-body systems.

Recently, fusion evaporation cross sections for the ^{64}Ni+^{64}Ni system have been measured down to the 10-nb level [2]. This experiment confirmed and improved the earlier data [3] for the same system and it extended the data to extreme sub-barrier energies, thus providing a challenge for the theoretical understanding of the fusion process between two open-shell nuclei. The primary observation was a *hindrance* of fusion in the ^{64}Ni+^{64}Ni system at extreme sub-barrier energies in comparison to reactions involving other nickel isotopes such as the ^{58}Ni+^{58}Ni system. Earlier coupled-channels calculations [4,5] failed to reproduce the data at the extreme sub-barrier energies.

Various hypotheses were developed for explaining the fusion hindrance phenomenon. In Ref. [6] the hindrance was attributed to the differing stiffness of nickel isotopes from nuclear structure effects. An excellent coupled-channels fit to the data was obtained by supplementing the effective N-N force used in the double-folding potential with a repulsive core to account for the nuclear incompressibility effects at the nuclear overlap, thus leading to a shallow potential pocket. However, Refs. [7,8] suggest that at such low energies the inner turning point of the heavy-ion potential is smaller than the touching point $r_t = R_1 + R_2$. Thus the validity of the frozen-density approximation used in Ref. [6] becomes questionable. These authors have proposed a two-step model for fusion in which the effects of neck formation are approximately included [7].

The theoretical analysis of the fusion data generally involves the determination of a phenomenological ion-ion potential such as the Bass model [9,10], the proximity potential [11–14], or potentials obtained via the double-folding method [15–18]. Subsequently, the actual fusion cross section is calculated by either using barrier penetration models [10,17,19,20], or the coupled-channel method [4,5,21–23]. The latter includes various excitations of the target and/or projectile using the coupled-channel formalism [4,23], as well as the inclusion of neutron transfer, and can be consistently applied at energies above and below the barrier [20]. Effectively, the inclusion of each additional excitation leads to a modification of the original inert core ion-ion potential, resulting in a series of effective barriers. One common physical assumption used in many of these calculations is the use of the frozen density or the sudden approximation. In this approximation the nuclear densities are unchanged during the computation of the ion-ion potential as a function of the internuclear distance. Furthermore, the coupled-channel approaches are based on properties of low-lying collective states in the projectile and target nuclei such as excitation energies and $B(EL)$ values, which are usually taken from experiment. These may accurately represent the early stages of the collision process, but the collective excitations are expected to change as the two ions strongly interact. Although these methods provide a useful and productive means for quantifying multitudinous reaction data it is desirable to include dynamical effects and make contact with the microscopic theories of nuclear structure and reactions.

Recently, we have developed a microscopic approach for calculating heavy-ion interaction potentials that incorporates all of the dynamical entrance channel effects included in the time-dependent Hartree-Fock (TDHF) description of the collision process [24]. These effects include the neck formation, particle exchange, internal excitations, and deformation effects to all orders, as well as the effect of nuclear alignment for deformed systems. The method is based on the TDHF evolution of the nuclear system coupled with density-constrained Hartree-Fock calculations to obtain the ion-ion interaction potential. Preliminary calculations for the ^{64}Ni+^{132}Sn system highlighted the importance of dynamical deformation effects [25,26]. Here we give a completed study of fusion cross sections using this formalism.

In the next section we will summarize some theoretical aspects of the density-constrained TDHF theory along with

methods to incorporate dynamical alignment into our calculations, as well as the method used to calculate cross sections from the resulting barriers. In Sec. III we present interesting aspects of the reaction dynamics and compare our results with experiment and other calculations. In Sec. IV we summarize our conclusions.

II. THEORETICAL METHODS

A. Density-constrained TDHF method

For the calculations of dynamical potential barriers for the ^{64}Ni+^{64}Ni system we have used the density-constrained TDHF (DC-TDHF) method. Further details of the method can be found in Ref. [24]; here we give a short overview.

The *density constraint* is a novel numerical method that was developed in the mid 1980s [27,28] and was used to provide a microscopic description of the formation of shape resonances in light systems [28]. In this approach the TDHF time evolution takes place with no restrictions. At certain times during the evolution the instantaneous density is used to perform a static Hartree-Fock minimization while holding the total density constrained to be the instantaneous TDHF density. In essence, this provides us with the TDHF dynamical path in relation to the multidimensional static energy surface of the combined nuclear system. Since we are constraining the total density all moments are simultaneously constrained. The numerical procedure for implementing this constraint and the method for steering the solution to $\rho_{\mathrm{TDHF}}(\mathbf{r}, t)$ is discussed in Refs. [27,28]. The convergence property is as good if not better than in the traditional constrained Hartree-Fock calculations with a constraint on a single collective degree of freedom.

In Ref. [24] we have shown that the ion-ion interaction potential is given by

$$V(R) = E_{\mathrm{DC}}(R) - E_{A_1} - E_{A_2}, \tag{1}$$

where E_{DC} is the density-constrained energy at the instantaneous separation $R(t)$ and E_{A_1} and E_{A_2} are the binding energies of the two nuclei obtained with the same effective interaction. We would like to emphasize again that this procedure does not affect the TDHF time evolution and contains no *free parameters* or *normalization*. In practice, TDHF runs are initialized with energies above the Coulomb barrier and in Ref. [24] we have shown that there is no appreciable energy dependence to the barriers obtained via the density-constrained TDHF method. The separation coordinate R is the distance between the centers of mass of the two nuclei.

In addition to the ion-ion potential it is also possible to obtain the coordinate-dependent mass $M(R)$ by using conservation of energy:

$$M(R) = \frac{2[E_{\mathrm{c.m.}} - V(R)]}{\dot{R}^2}, \tag{2}$$

where the collective velocity $\dot{R}$ is directly obtained from the TDHF evolution and the potential $V(R)$ from the density constraint calculations. In calculating fusion cross sections by solving the Schrödinger equation we can either use this coordinate-dependent mass or transfer the effects of this mass to the ion-ion potential using the well-known coordinate scale transformation [29]

$$d\bar{R} = \left(\frac{M(R)}{\mu}\right)^{\frac{1}{2}} dR. \tag{3}$$

As a result of this transformation all of the effects of the coordinate-dependent mass are transferred to the scaled potential while the reduced mass μ remains constant at its asymptotic value.

B. Fusion for deformed nuclei

The heavy-ion interaction potential between two deformed nuclei depends on the distance vector between their centers of mass, $\mathbf{R}$, and on the relative orientation of their intrinsic principal axis systems, which may be described in terms of three Euler angles (α, β, γ) per nucleus; that is, in the most general case we have

$$V = V(\mathbf{R}, \alpha_1, \beta_1, \gamma_1, \alpha_2, \beta_2, \gamma_2). \tag{4}$$

The expression for V can be simplified if the intrinsic nuclear density distributions are axially symmetric; in this case, the potential does not depend on the Euler angles γ_1, γ_2, which describe rotations about the symmetry axes. If we put, for convenience, the distance vector in the z-direction, $\mathbf{R} = R\mathbf{e}_z$, the potential between two deformed axially symmetric nuclei has the structure

$$V = V(R, \beta_1, \beta_2, \Delta\alpha). \tag{5}$$

The heavy-ion interaction potential is calculated with the DC-TDHF method for a given set of orientation angles β_1, β_2, and $\Delta\alpha$. Fortunately, test calculations using the double-folding method described in Ref. [18] reveal that the dependence on the Euler angle $\Delta\alpha$ is negligible in our case: For example, at fixed Euler angles $\beta_1 = 30^\circ$ and $\beta_2 = 120^\circ$ we find potential barrier values of 94.26, 94.28, and 94.30 MeV for $\Delta\alpha = 0^\circ, 45^\circ$, and 90°, respectively. This variation is much smaller than the variation with the Euler angles β_1 and β_2, which amount to several MeV. In the DC-TDHF calculations of the heavy-ion potential we therefore put $\Delta\alpha = 0$. In Fig. 1 we show the definition of the angles β_1 and β_2 for two oblate nuclei. To calculate the total fusion cross section at energy $E_{\mathrm{c.m.}}$, we first consider the partial cross section for given initial orientations

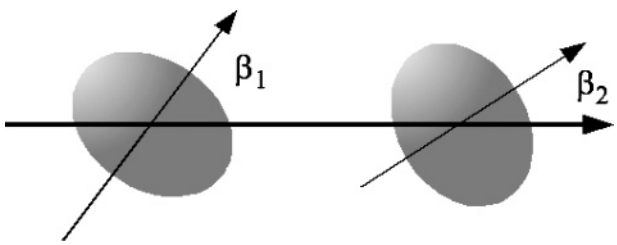

FIG. 1. Orientation angles β_1 and β_2 of the oblate Ni nuclei with respect to the collision axis.

(β_1, β_2) of the two nuclei, which is given by

$$\sigma(E_{\text{c.m.}}, \beta_1, \beta_2) = \frac{\pi}{k_0^2} \sum_{L=0}^{\infty} (2L+1) T_L(E_{\text{c.m.}}, \beta_1, \beta_2), \quad (6)$$

with $k_0 = \sqrt{2\mu E_{\text{c.m.}}}$. The fusion barrier penetrabilities $T_L(E_{\text{c.m.}}, \beta_1, \beta_2)$ are obtained by numerical integration of the two-body Schrödinger equation by using the incoming wave boundary condition (IWBC) method [21,30]:

$$\left[\frac{-\hbar^2}{2\mu} \frac{d^2}{dR^2} + \frac{L(L+1)\hbar^2}{2\mu R^2} + V(R, \beta_1, \beta_2) - E \right] \psi = 0,$$

where the quantity $V(R, \beta_1, \beta_2)$ denotes the heavy-ion potential obtained via the DC-TDHF method. For the numerical implementation we have followed the procedure for the coupled-channel code CCFULL described in Ref. [23]. In IWBC it is assumed that once the minimum of the potential is reached fusion will occur. In practice, the Schrödinger equation is integrated from the potential minimum, R_{min}, where only an incoming wave is assumed, to a large asymptotic distance, where it is matched to incoming and outgoing Coulomb wave functions. The barrier penetration factor, $T_L(E_{\text{c.m.}}, \beta_1, \beta_2)$, is the ratio of the incoming flux at R_{min} to the incoming Coulomb flux at large distance.

Once the partial fusion cross sections [Eq. (6)] for given orientation angles (β_1, β_2) have been calculated, we have to take an average over all initial angular orientations of both nuclei:

$$\sigma(E_{\text{c.m.}}) = \int_0^{\pi} \sin(\beta_1) d\beta_1 \int_0^{\pi} \sin(\beta_2) d\beta_2 \times \frac{d^2 P(E_{\text{c.m.}}, \beta_1, \beta_2)}{\sin(\beta_1) d\beta_1 \sin(\beta_2) d\beta_2} \sigma(E_{\text{c.m.}}, \beta_1, \beta_2),$$

where $d^2 P(E_{\text{c.m.}}, \beta_1, \beta_2)$ represents the alignment probability for both deformed nuclei. Details of the dynamic alignment formalism are presented in Ref. [31]. We give here a brief summary: For a given incident energy $E_{\text{c.m.}}$ we carry out a semiclassical Coulomb excitation calculation of the dominant collective levels of the deformed nucleus. The energy levels and EL-transition matrix elements for ^{64}Ni are taken from experimental data [32]: $E_{2+} = 1.346$ MeV, $E_{4+} = 2.610$ MeV, and $M(E2, 0+ \rightarrow 2+) = -27.0e\,\text{fm}^2$ (oblate deformation). The Coulomb excitation calculation starts at very large internuclear distances (about 1500 fm) when both nuclei may be presumed to be in their respective ground states and stops at the ion-ion separation distance $R(t_0)$ (about 16 fm). The Coulomb excitation amplitudes determine the probability distribution of initial orientations. Using the dominant monopole-multipole part of the Coulomb interaction, the orientation probability factorizes as follows:

$$\frac{d^2 P(E_{\text{c.m.}}, \beta_1, \beta_2)}{\sin(\beta_1) d\beta_1 \sin(\beta_2) d\beta_2} = \frac{dP_1(E_{\text{c.m.}}, \beta_1)}{\sin(\beta_1) d\beta_1} \frac{dP_2(E_{\text{c.m.}}, \beta_2)}{\sin(\beta_2) d\beta_2}.$$

In the special case of no preferential alignment (i.e., all initial orientation angles are equally likely), this factor reduces to

$$\left. \frac{d^2 P(E_{\text{c.m.}}, \beta_1, \beta_2)}{\sin(\beta_1) d\beta_1 \sin(\beta_2) d\beta_2} \right|_{\text{noalign}} \longrightarrow \frac{1}{4}.$$

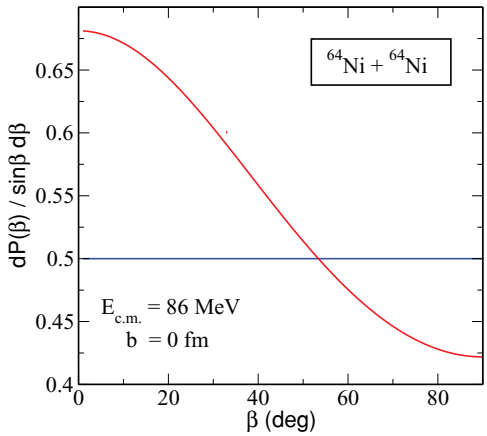

FIG. 2. (Color online) Dynamic alignment resulting from Coulomb excitation of ^{64}Ni. Shown is the orientation probability as a function of the Euler angle β in a central collision at internuclear distances $R = 1500$ fm (blue curve) and at $R = 16$ fm (red curve).

In Fig. 2 we show the differential alignment probability as a function of the Euler angle β used in our calculations.

III. RESULTS

We have carried out a number of TDHF calculations with accompanying density constraint calculations to compute $V(R, \beta_1, \beta_2)$ given by Eq. (1). A detailed description of our new three-dimensional unrestricted TDHF code has recently been published in Ref. [33]. The code was modified to self-consistently generate initial states for ^{64}Ni with different orientations. For the effective interaction we have primarily used the Skyrme SLy5 force [34], including all of the time-odd terms. In this case the ^{64}Ni nucleus is essentially oblate, having a quadrupole moment of -0.45 b. This is also confirmed by other calculations [35,36].

All of our TDHF calculations were done at an initial energy of $E_{\text{c.m.}} = 98$ MeV and separation $R(t_0) = 16$ fm. We have tested the convergence of ion-ion separation by performing a DC-TDHF calculation starting from $R(t_0) = 30$ fm and found no numerically significant difference between the two results. As we have reported in Ref. [24] the potential barriers obtained from the DC-TDHF method are not sensitive to the initial energy (above the barrier). We have tested this again by running a few orientations at 112 MeV and did not observe any appreciable difference. In Fig. 3 we show the barriers obtained for limiting orientations of the ^{64}Ni nuclei, as well as the effect of the coordinate-dependent mass, $M(R)$, on the heavy-ion potentials (dashed curves). We have also calculated these limiting barriers using other effective interactions, SkM* [37] and SLy4 [34], with essentially no difference.

The physical picture that emerges from the barriers shown in Fig. 3 is that the total fusion cross section strongly depends on the deformation phase space. It also shows the fallacy of the often-used statement that a certain energy is *sub-barrier*, which stems from spherical systems that can be studied by using a single barrier. For deformed systems this is dependent on the orientation of the nuclei. For the ^{64}Ni+^{64}Ni system the only

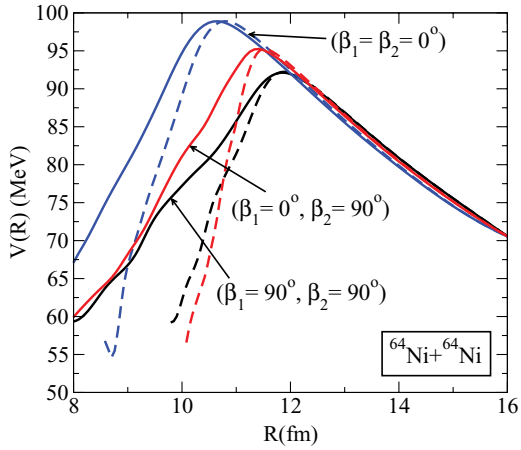

FIG. 3. (Color online) Potential barriers, $V(R, \beta_1, \beta_2)$, obtained from density-constrained TDHF calculations for the ^{64}Ni+^{64}Ni system. The Euler angles β_1 and β_2 indicate different orientations of the deformed ^{64}Ni nucleus. Solid curves are calculated with constant reduced mass; the dashed curves show the corresponding barriers incorporating the effects of the coordinate-dependent mass.

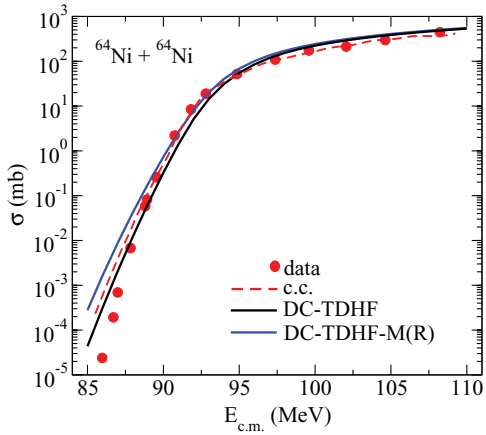

FIG. 4. (Color online) Total fusion cross section as a function of $E_{\text{c.m.}}$. Shown are the experimental data (filled red circles) and the coupled-channel calculation from Ref. [2] (red dashed curve) and fusion cross sections calculated with the density-constrained TDHF method using the SLy5 force with constant reduced mass (solid black line) and with coordinate-dependent mass (solid blue line).

truly sub-barrier energies are those below the lowest potential barrier corresponding to the $\beta_1 = \beta_2 = 90^\circ$ orientation, about $E_{\text{c.m.}} = 92$ MeV. The fusion cross sections corresponding to energies above the lowest barrier will be dominated by it since above-barrier cross sections are much larger than the below-barrier ones.

For the calculation of barrier distributions as a function of the orientation angles β_1 and β_2 we have chosen an angular spacing of $\Delta\beta = 10^\circ$. In principle this requires 400 DC-TDHF calculations, which would be very time consuming. However, one can show that some of the orientations are equivalent to each other. One major assumption we have made is to assume the equality of the angular intervals $(0, \pi/2)$ and $(\pi/2, \pi)$, which is not exactly correct when both nuclei are deformed. To assure that this approximation does not affect the lowest energy cross sections (primarily determined by the lowest barrier) we have explicitly calculated those angles that would have appreciable contribution at these energies. In total we have computed 20 potential barriers corresponding to various orientations for the SLy5 force. In principle even this may not be necessary since all of the barriers must fall between the limiting cases shown in Fig. 3. Although actual calculations show that a constant angular interval $\Delta\beta$ does not always lead to equally spaced barriers, such an extrapolation has a minimal effect on the actual cross section calculations. We have confirmed this by generating such barriers from the limiting barriers using a numerical averaging procedure and calculating the fusion cross section.

In Fig. 4 we show the total DC-TDHF fusion cross section as a function of the center-of-mass energy using the SLy5 force with constant reduced mass (solid black curve) and with coordinate-dependent mass (solid blue curve). Also shown are the experimental data (filled circles) and the coupled-channels calculations of Ref. [2] (dashed red line). Results for SLy4 and SkM* interactions are indistinguishable from the SLy5 result. We observe that the DC-TDHF calculations, which contain no parameters or normalization, accurately reproduce the fusion cross sections for all energies except for energies $E_{\text{c.m.}} \leqslant 87$ MeV. The cross sections calculated with a coordinate-dependent mass (solid blue line) show an improvement in the intermediate energy range but overpredict the data at lower energies. We believe that the small deviations at higher energies are largely due to the symmetry assumptions made in alignment averaging. As we stated earlier this is not the case for the lowest energies as these were explicitly done without symmetry assumptions.

To better examine the evolution of the nuclear density, in Fig. 5 we have plotted the nuclear density at four special internuclear distances R for the $\beta_1 = \beta_2 = 90^\circ$ initial orientation. Frame (a) corresponds to the nuclear density at the outer turning point of the ion-ion potential ($R = 13.1$ fm) at $E_{\text{c.m.}} \leqslant 86$ MeV. Frame (b) of Fig. 5 shows the total density at the ion-ion separation of $R = 11.0$ fm, which approximately corresponds to the location of the inner turning point at $E_{\text{c.m.}} \leqslant 86$ MeV. The mass density distribution of ^{64}Ni predicted by the Skyrme-HF calculation shows that the outer skin and the inner core have different orientations. Therefore there is an ambiguity in the definition of "nuclear orientation." At low beam energies, the sub-barrier fusion cross section is dominated by the lowest potential barrier, which according to Fig. 3 corresponds to Euler angles $\beta_1 = \beta_2 = 90^\circ$ (defined with respect to the outer skin). In examining the density distribution of the dinuclear system as a function of the internuclear distance R in Fig. 5, we find that the skin and the core regions of the matter distribution have different orientations at distances R larger than 10 fm. At around $R = 10$ fm, inside the pocket, the nuclear core rotates and aligns with the total nuclear density. In frame (c) we show this at $R = 9.5$ fm. The last frame (d) shows the nuclear density at the potential minimum, which occurs around $R = 8.0$ fm. We have investigated the microscopic origin of the difference between core orientation and skin orientation in the density

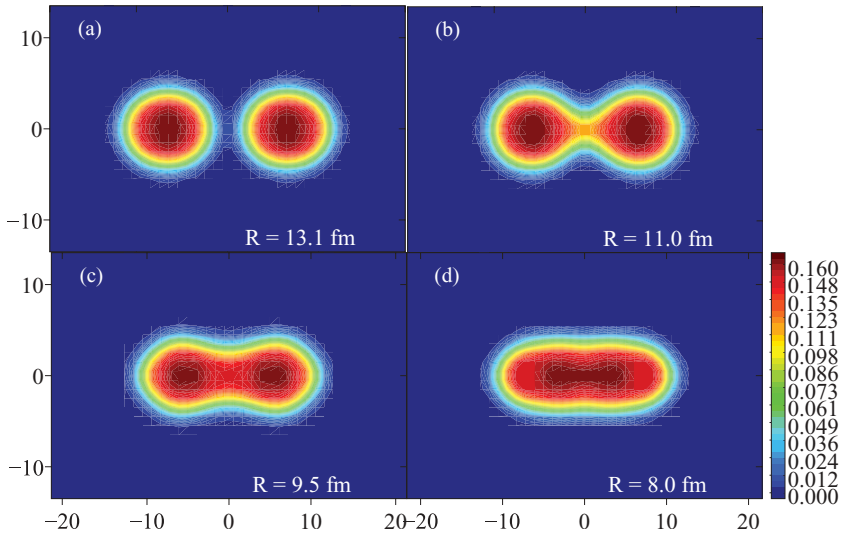

FIG. 5. (Color online) Density contours in the x-z plane for the TDHF time evolution of the ^{64}Ni+^{64}Ni system. Initially both nuclei are oriented with angles $\beta_1 = \beta_2 = 90^\circ$ at a center-of-mass energy of $E_{\text{c.m.}} = 98$ MeV. The values for the ion-ion separation R correspond to special points along the potential barrier at the lowest experimental energy of $E_{\text{c.m.}} = 86$ MeV: (a) outer turning point, (b) inner turning point, (c) reorientation of the core, and (d) potential minimum.

of ^{64}Ni. For this purpose, we have examined the quadrupole moments q_{20} of all single-particle states, both for neutrons and for protons. We find that the occupied states in this nucleus have single-particle quadrupole moments that are predominantly of the same sign (negative for our choice of quantization axis). However, we find that there are two deeply bound low-angular-momentum $j_z = \pm 1/2$ states with large opposite (positive) quadrupole moment: The neutron single-particle state at $E = -21.2$ MeV has a q_{20} value of $+11.1$ fm^2 and the corresponding proton state at $E = -16.6$ MeV has a quadrupole moment of $+11.4$ fm^2. To link the core orientation to a physical observable we have computed the quadrupole moments of the individual nuclei with respect to their centers during the collision. We observe that as the two nuclei approach the touching configuration their respective quadrupole moments increase because of their rotating cores.

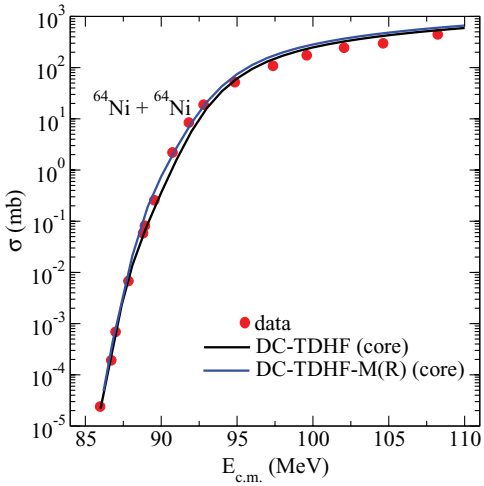

FIG. 6. (Color online) Total fusion cross section as a function of $E_{\text{c.m.}}$. Shown are the experimental data (filled red circles) and the density-constrained TDHF cross sections using the core orientation with the SLy5 force for the lowest energy cross sections with constant reduced mass (solid black line) and with coordinate-dependent mass (solid blue line).

A similar phenomenon was observed in macroscopic-microscopic model calculations of the ^{64}Ni + ^{208}Pb fusion barrier [38]. In their work the authors took into account the projectile deformation effect on the fusion barrier. They find that the original oblate deformation of the ^{64}Ni projectile turns into a large prolate deformation caused by the attractive nuclear force as the target and projectile come closer. The instability develops before touching because the attractive short-range nuclear force overcomes the repulsive Coulomb force and the shape-stabilizing effect of shell structure.

Based on these considerations let us hypothesize that, at low bombarding energies, the core nucleons play a more important role than the outer skin. Making this assumption, we find that by using the core orientation angle rather than the skin orientation in the angle-averaging procedure for the lowest beam energies ($E_{\text{c.m.}} \leqslant 87$ MeV) we are able to reproduce the measured fusion cross sections (see Fig. 6). Again, the calculations were carried out with constant reduced mass and coordinate-dependent mass, as shown by the black and blue curves in Fig. 6, respectively. The coordinate-dependent mass improves the intermediate energy cross sections. Although the coordinate-dependent mass affects the orientation-angle-dependent barriers significantly (Fig. 3), the impact on the fusion cross section is reduced by the $\sin(\beta)d\beta$ factors in the orientation-angle-averaging procedure when core orientation angles are used.

IV. CONCLUSIONS

As we investigate fusion reactions involving neutron-rich and deformed nuclei it is apparent that an understanding of the structure of these nuclei is crucial to the description of the reaction dynamics. For these nuclei various effects, such as inelastic excitations, particle transfer, and other dynamical effects, lead to substantial modification of the naive potential barrier calculations, in which an inert core and no dynamics are assumed. Consequently, the definition of *sub-barrier* fusion becomes ambiguous since it is difficult to determine the barrier *a priori*.

We have performed density-constrained TDHF calculations of fusion cross sections for the ^{64}Ni+^{64}Ni system. Our results agree well with the measured data despite having no adjustable parameters. This indicates that many of the reaction dynamics are included in the TDHF evolution of the nuclear density. It would be truly amazing if a fully microscopic calculation that contains no free parameters or normalization, such as the DC-TDHF method, would be able to reproduce the measured fusion cross sections better than the coupled-channel calculations. The main purpose of the fully microscopic calculations is to gain insight into the reaction dynamics and to investigate those degrees of freedom that are completely absent from methods that use a phenomenological frozen-density approximation. However, the DC-TDHF calculations show a lot of promise for the microscopic description of heavy-ion fusion as better and better effective interactions are developed.

We have further investigated fusion cross sections at deep sub-barrier energies. In the absence of a true many-body tunneling approach to nuclear fusion it is difficult to envision the dynamical formation of the potential barrier at very deep sub-barrier energies. As we go further down in energy the inner turning point of the ion-ion potential involves larger overlaps among the participating nuclei. Consequently, core nucleons may play a more dominant role in dynamically building up the potential barrier. In the case of $\beta_1 = \beta_2 = 90^\circ$, corresponding to the lowest potential barrier, we observed that the nuclear core has a different orientation from the total nuclear density. Based on this observation we have speculated that at the lowest energies it may make sense to use the orientation of the core rather than the nuclear surface. This core orientation effect allows us to reproduce the experimental cross sections at the lowest energies.

ACKNOWLEDGMENTS

This work has been supported by the U.S. Department of Energy under Grant No. DE-FG02-96ER40963 with Vanderbilt University.

[1] *Opportunities in Nuclear Science, A Long-Range Plan for the Next Decade*, DOE/NSF Nuclear Science Advisory Committee, April 2002, http://www.sc.doe.gov/henp/np/nsac/docs/LRP_5547_FINAL.pdf.
[2] C. L. Jiang *et al.*, Phys. Rev. Lett. **93**, 012701 (2004).
[3] M. Beckerman, M. Salomaa, A. Sperduto, J. D. Molitoris, and A. DiRienzo, Phys. Rev. C **25**, 837 (1982).
[4] H. Esbensen, Prog. Theor. Phys. Suppl. **154**, 11 (2004).
[5] H. Esbensen, Phys. Rev. C **72**, 054607 (2005).
[6] Ş. Mişicu and H. Esbensen, Phys. Rev. Lett. **96**, 112701 (2006).
[7] T. Ichikawa, K. Hagino, and A. Iwamoto, Phys. Rev. C **75**, 057603 (2007).
[8] T. Ichikawa, K. Hagino, and A. Iwamoto, Phys. Rev. C **75**, 064612 (2007).
[9] R. Bass, Nucl. Phys. **A231**, 45 (1974).
[10] R. Bass, *Nuclear Reactions with Heavy Ions* (Springer Verlag, New York, 1980).
[11] J. Blocki, J. Randrup, W. J. Swiatecki, and C. F. Tsang, Ann. Phys. (NY) **105**, 427 (1977).
[12] J. Randrup and J. S. Vaagen, Phys. Lett. **B77**, 170 (1978).
[13] M. Seiwert, W. Greiner, V. E. Oberacker, and M. J. Rhoades-Brown, Phys. Rev. C **29**, 477 (1984).
[14] J. R. Birkelund and J. R. Huizenga, Phys. Rev. C **17**, 126 (1978).
[15] G. R. Satchler and W. G. Love, Phys. Rep. **55**, 183 (1979).
[16] G. Bertsch, J. Borysowicz, H. McManus, and W. G. Love, Nucl. Phys. **A284**, 399 (1977).
[17] M. J. Rhoades-Brown and V. E. Oberacker, Phys. Rev. Lett. **50**, 1435 (1983).
[18] M. J. Rhoades-Brown, V. E. Oberacker, M. Seiwert, and W. Greiner, Z. Phys. A **310**, 287 (1983).
[19] N. Takigawa and G. F. Bertsch, Phys. Rev. C **29**, 2358 (1984).
[20] A. B. Balantekin and N. Takigawa, Rev. Mod. Phys. **70**, 77 (1998).
[21] S. Landowne and S. C. Pieper, Phys. Rev. C **29**, 1352 (1984).
[22] M. J. Rhoades-Brown and M. Prakash, Phys. Rev. Lett. **53**, 333 (1984).
[23] K. Hagino, N. Rowley, and A. T. Kruppa, Comput. Phys. Commun. **123**, 143 (1999).
[24] A. S. Umar and V. E. Oberacker, Phys. Rev. C **74**, 021601(R) (2006).
[25] A. S. Umar and V. E. Oberacker, Phys. Rev. C **74**, 061601(R) (2006).
[26] A. S. Umar and V. E. Oberacker, Phys. Rev. C **76**, 014614 (2007).
[27] R. Y. Cusson, P.-G. Reinhard, M. R. Strayer, J. A. Maruhn, and W. Greiner, Z. Phys. A **320**, 475 (1985).
[28] A. S. Umar, M. R. Strayer, R. Y. Cusson, P.-G. Reinhard, and D. A. Bromley, Phys. Rev. C **32**, 172 (1985).
[29] K. Goeke, F. Grümmer, and P.-G. Reinhard, Ann. Phys. (Leipzig) **150**, 504 (1983).
[30] G. H. Rawitscher, Phys. Rev. **135**, 605 (1964).
[31] A. S. Umar and V. E. Oberacker, Phys. Rev. C **74**, 024606 (2006).
[32] Evaluated Nuclear Structure Data File (ENSDF), National Nuclear Data Center, Brookhaven National Laboratory, http://www.nndc.bnl.gov/ensdf.
[33] A. S. Umar and V. E. Oberacker, Phys. Rev. C **73**, 054607 (2006).
[34] E. Chabanat, P. Bonche, P. Haensel, J. Meyer, and R. Schaeffer, Nucl. Phys. **A635**, 231 (1998); **A643**, 441(E) (1998).
[35] J. Dobaczewski, M. V. Stoitsov, and W. Nazarewicz, AIP Conf. Proc. **726**, 51 (2004).
[36] G. A. Lalazissis, S. Raman, and P. Ring, At. Data Nucl. Data Tables **71**, 1 (1999).
[37] J. Bartel, P. Quentin, M. Brack, C. Guet, and H. B. Hakansson, Nucl. Phys. **A386**, 79 (1982).
[38] T. Ichikawa, A. Iwamoto, P. Möller, and A. J. Sierk, Phys. Rev. C **71**, 044608 (2005).